

Formation of “Blanets” from Dust Grains around the Supermassive Black Holes in Galaxies

KEIICHI WADA,^{1,2,3} YUSUKE TSUKAMOTO,¹ AND EIICHIRO KOKUBO⁴

¹*Kagoshima University, Graduate School of Science and Engineering, Kagoshima 890-0065, Japan*

²*Ehime University, Research Center for Space and Cosmic Evolution, Matsuyama 790-8577, Japan*

³*Hokkaido University, Faculty of Science, Sapporo 060-0810, Japan*

⁴*National Astronomical Observatory of Japan, Mitaka 181-8588, Japan*

ABSTRACT

In Wada, Tsukamoto, and Kokubo (2019), we proposed for the first time that a new class of planets, *blanets*, can be formed around supermassive black holes (SMBHs) in the galactic center. Here, we investigate the dust coagulation processes and physical conditions of the blanet formation outside the snowline ($r_{snow} \sim$ several parsecs) in more detail, especially considering the effect of the radial drift of the dust aggregates. We found that a dimensionless parameter $\alpha = v_t^2/c_s^2$, where v_t is the turbulent velocity and c_s is the sound velocity, describing the turbulent viscosity should be smaller than 0.04 in the circumnuclear disk to prevent the destruction of the aggregates due to collision. The formation timescale of blanets τ_{GI} at r_{snow} is, $\tau_{GI} \simeq 70\text{--}80$ Myr for $\alpha = 0.01\text{--}0.04$ and $M_{BH} = 10^6 M_\odot$. The mass of the blanets ranges from $\sim 20M_E$ to $3000M_E$ in $r < 4$ pc for $\alpha = 0.02$ (M_E is the Earth mass), which is in contrast with $4M_E\text{--}6M_E$ for the case without the radial drift. Our results suggest that blanets could be formed around relatively low-luminosity AGNs ($L_{bol} \sim 10^{42}$ erg s⁻¹) during their lifetime ($\lesssim 10^8$ yr).

1. INTRODUCTION

There is enough evidence suggesting that planets are formed in the circumstellar disks around stars. However, stars might not be the only site for planet formation. Recently, in Wada, Tsukamoto, and Kokubo (2019) (hereafter Paper I), we claimed a new class of “planets”¹ that orbit around super-massive black holes (SMBHs) in galactic centers. Paper I theoretically investigated the growth processes of planets, from sub-micron-sized icy dust monomers to Earth-sized bodies outside the snowline in a circumnuclear disk around a SMBH, typically located several parsecs from the SMBHs. As is the case in a protostellar disk, in the early phase of the dust evolution,

Corresponding author: Keiichi Wada
wada@astrophysics.jp

¹ Here, we merely call massive rocky/icy objects orbiting around a central gravity source as “planets”.

low-velocity collisions between dust particles promote sticking; therefore, the internal density of the dust aggregates decreases with growth (Okuzumi et al. 2012; Kataoka et al. 2013). When the size of porous dust aggregates reaches 0.1–1 cm, the collisional and the gas-drag compression become effective, and as a result, the internal density stops decreasing. Once 10–100 m sized aggregates are formed, they decouple from gas turbulence, and as a result, the aggregate layer becomes gravitationally unstable (Michikoshi, & Kokubo 2016, 2017), leading to the formation of “planets” due to the fragmentation of the layer, with ten times the mass of the earth. The objects orbit the SMBHs with an orbital time of $10^5 - 10^6$ years. To distinguish them from standard planets, we hereafter call these hypothetical astronomical objects *blanets*².

The results reported in Paper I, however, have two major limitations. One is that the collisional velocity between the dust aggregates might become too large ($>$ several 100 m s^{-1} at the Stokes parameter, $S_t \sim 1$). And if the collisional velocity is that large, rather than growing, the aggregates might get destroyed. In Paper I, we used the numerical experiments conducted by Wada et al. (2009)³ on the collisions between the dust aggregates, wherein the critical collisional velocity (v_{crit}) scales with the mass m_d of the dust aggregates, as $v_{crit} \propto m_d^{1/4}$. However, this is correct only for the head-on collisions, as stated in the paper. Moreover, Wada et al. (2009, 2013) showed that the growth efficiency of the dust aggregates depends on the impact parameter of the collisions, and as a result, v_{crit} does not strongly depend on the mass of the dust aggregates, if off-set collisions are taken into account. They concluded that $v_{crit} \simeq 80 \text{ m s}^{-1}$ for the ice monomers⁴. This low critical velocity is also one of the obstacles in the planet formation in circumstellar disks. In this follow-up paper, we adopt $v_{crit} \simeq 80 \text{ m s}^{-1}$ as a constraint on the growth of the dust aggregates.

Another limitation of Paper I is that the size of dust aggregates a_d and collisional velocity Δv show runaway growth in the collisional compression phase around $S_t \sim 1$. However, this rapid growth would not be realistic if a more natural treatment of the internal density of the dust is considered (§2.2.1, see also §3).

Moreover, there is a critical process that may promote blanet formation. In paper I, we did not take into account the radial drift of the dust particles as the first approximation. The radial velocity of the dust $v_{r,d}$ relative to the gas (Weidenschilling 1977; Tsukamoto et al. 2017) is $v_{r,d} \sim S_t \eta v_K$, and $\eta \sim (c_s/v_K)^2$, where c_s is the gas isothermal sound velocity and v_K is the Keplerian rotational velocity. In the circumnuclear disk around a SMBH, initially $S_t \eta \sim 10^{-4} - 10^{-3}$. Then the drift time of the dust particle $t_{drift} \sim r/v_{r,d} \sim 5 - 50(M_{BH}/10^7 M_\odot)^{1/2}(r/1 \text{ pc})^{1/2} \text{ Myr}$. This is not negligibly small for the lifetime of the active galactic nucleus (AGN), i.e.,

² This does not necessarily mean a simple abbreviation of “black hole planet”, because this new class of objects does not resemble the planets in the solar system nor any known exoplanet systems, in a sense that a swarm of super-Earth mass objects are orbiting around the central gravity source. See also §4.2.

³ Note that Wada et al. (2009) and Wada et al. (2013) were written by Koji Wada and his collaborators, not by the first author of this paper.

⁴ Here, we suppose water ice (Sato et al. 2016). In fact, the presence of H_2O in AGNs is suggested by maser observations (e.g., Greenhill et al. 2003), and by chemical models (e.g., Wada et al. 2016). Note that v_{crit} is much smaller ($\sim 1 \text{ m s}^{-1}$) for silicate monomers (Wada et al. 2009). Therefore, we here consider dust evolution outside the snowline.

$10^7 - 10^8$ yr. In this paper, we investigate the effects of the radial drift of the dust particles.

The remainder of this paper is organized as follows. In §2, we describe the models for the dust evolution and its application to the circumnuclear region. In §3, we show the results of the models with and without the radial drift of the dust particles. In §4, we discuss how the maximum collisional velocity and the formation timescale of blanets depend on the parameters α and M_{BH} . We also discuss the expected mass of the blanets and their radial distribution. Finally, we summarize the results in §5.

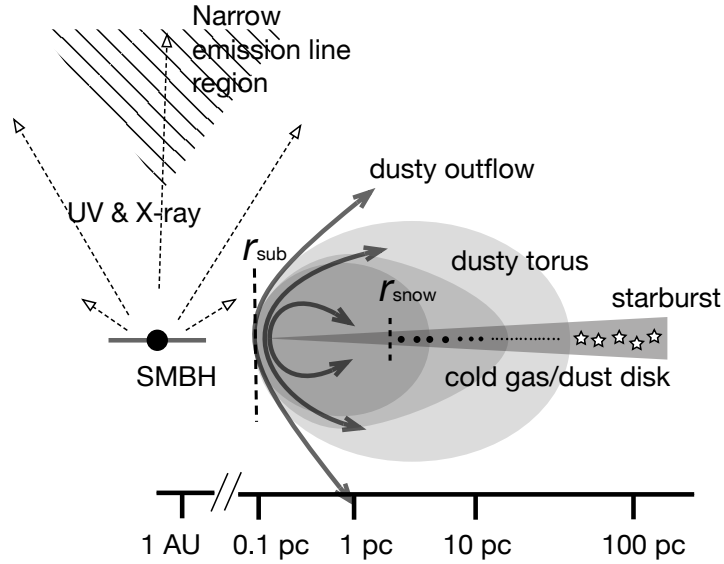


Figure 1. A schematic picture of the Active Galactic Nucleus (AGN) and the circumnuclear disk.

2. MODELS

2.1. The region of “blanet formation”

Here we briefly summarize the concept of dust evolution around SMBHs, as discussed in Paper I. Figure 1 shows a schematic of the active galactic nucleus (AGN) and the circumnuclear disk. A SMBH (with a mass of $10^6 - 10^{10} M_{\odot}$) is surrounded by an accretion disk, which radiates enormous energy (the bolometric luminosity is $\sim 10^{42} - 10^{45} \text{ erg s}^{-1}$), mostly as ultra-violet and X-rays. The dust particles in the central $r < r_{sub}$ are sublimated by the radiation from the accretion disk around the SMBH. The radius depends on the AGN luminosity:

$$r_{sub} \simeq 1.3 \text{ pc} \left(\frac{L_{UV}}{10^{46} \text{ erg s}^{-1}} \right)^{0.5} \left(\frac{T_{sub}}{1500 \text{ K}} \right)^{-2.8} \left(\frac{a_d}{0.05 \mu\text{m}} \right)^{-1/2}. \quad (1)$$

where L_{UV} is the ultra-violet luminosity of the AGN, and a_d is the dust size (Barvainis 1987). The radiation forms conical ionized gas (narrow emission-line region) and

also contributes to producing the outflows of the dusty gas and torus (Wada 2012; Wada et al. 2018; Izumi et al. 2018). In the mid-plane of the torus, cold, dense gas forms a thin disk, where icy dust particles can be present beyond the snowline r_{snow} (see §2.4).

We introduce a free parameter $\alpha \equiv v_t^2/c_s^2$, where c_s is the gas sound velocity and v_t is the turbulent velocity, to represent strength of the kinematic viscosity due to the turbulence (e.g., Ormel, & Cuzzi 2007, see also eqns. (7) and (8)). In the circumnuclear disk in AGNs, the value of α is highly uncertain⁵. Therefore, we here treat α as a free parameter to check how it alters the results, especially the maximum collisional velocity between the dust aggregates and the onset of the gravitational instability of the dust disk.

In contrast to the dust coagulation process in the circumstellar disks (Weidenschilling 1977), the drag between dust particles and gas obeys the Epstein law. The aggregate's size (a_d) is always much smaller than the mean free path of the gas, $\lambda_g \sim 10^{12} \text{ cm}(\sigma_{mol}/10^{-15} \text{ cm}^2)^{-1}(n_{mol}/10^3 \text{ cm}^{-3})^{-1}$, where σ_{mol} and n_{mol} are the collisional cross-section and number density of the gas, respectively.

2.2. Evolution of dust aggregates in each stage

The model for the growth of dust particles here is based on the elementary processes found around stars. The evolution of dust particles is divided into four stages as described below.

2.2.1. Hit-and-Stick stage

If the dust aggregates grow through ballistic cluster-cluster aggregation (BCCA), the internal structure of the aggregate should be porous (i.e., the internal density is much smaller than the monomer's density: $\rho_{int} \ll \rho_0$), and its fractal dimension is $D \simeq 1.9$ (Mukai et al. 1992; Okuzumi et al. 2009). This is called the *hit-and-stick* stage (Okuzumi et al. 2012; Kataoka et al. 2013), and the internal density is given by

$$\rho_{int} = \rho_0 \left(\frac{m_d}{m_0} \right)^{1-3/D}, \quad (2)$$

where m_d is the mass of the aggregate, and m_0 is the monomer's mass. We assume that $m_0 = 10^{-15} \text{ g}$ and $\rho_0 = 1 \text{ g cm}^{-3}$.

The growth rate for m_d is

$$\frac{dm_d}{dt} = \frac{2\sqrt{2\pi} \Sigma_d a_d^2 \Delta v}{H_d}, \quad (3)$$

where Δv is collision velocity between the aggregates, and H_d is the scale height of the dust disk as given in (Youdin, & Lithwick 2007; Tsukamoto et al. 2017);

⁵ In AGNs, the turbulence could be generated by various mechanisms; e.g., the magneto-rotational instability (Kudoh et al. 2020), the self-gravity (Shlosman, & Begelman 1987), the radiation-driven fountain (Wada 2012), and the stellar feedback (Wada & Norman 2002).

$$H_d = \left(1 + \frac{S_t}{\alpha} \frac{1 + 2S_t}{1 + S_t}\right)^{-1/2} H_g, \quad (4)$$

where $H_g = c_s/\Omega_K$ is the scale height of the gas disk, and S_t is the Stoke parameter, i.e., the normalized stopping time is defined as $S_t \equiv t_{stop}/t_L$ with the eddy turn over time t_L . Here we suppose that $t_L = \Omega_K^{-1}$ and

$$S_t = \frac{\pi \rho_{int} a_d}{2\Sigma_g}. \quad (5)$$

The collision velocity between aggregates Δv for $S_t < 1$ can be divided into two regimes (Ormel, & Cuzzi 2007): regime I) $t_s \ll t_\eta = t_L Re^{-1/2}$, and regime II) $t_\eta \ll t_s \ll \Omega_K^{-1}$. Here the Reynolds number, $Re \equiv \alpha c_s^2/(\nu_{mol}\Omega_K)$ with the molecular viscosity $\nu_{mol} \sim \frac{1}{2}c_s\lambda_g$ is

$$Re \approx 3 \times 10^4 \left(\frac{M_{BH}}{10^6 M_\odot}\right)^{-1/2} \left(\frac{r}{1 \text{ pc}}\right)^{3/2} c_{s,1}^{-1} Q_g \left(\frac{\gamma_{Edd}}{0.01}\right), \quad (6)$$

where Q_g is the Toomre's Q -value for the gas disk and γ_{Edd} is the Eddington ratio for the AGN. For the hit-and-stick stage, $S_t \ll Re^{-1/2}$, then for the regime I,

$$\Delta v_I \simeq \sqrt{\alpha} c_s R_e^{1/4} |S_{t,1} - S_{t,2}| = C_I \sqrt{\alpha} c_s R_e^{1/4} S_t, \quad (7)$$

where $S_{t,1}$ and $S_{t,2}$ are Stokes numbers of the two colliding particles, and C_I is a constant of the order of unity (Sato et al. 2016). For regime II, on the other hand,

$$\Delta v_{II} \simeq v_L \sqrt{t_{stop}/t_L} \simeq \sqrt{\alpha S_t} c_s \quad (8)$$

where v_L is velocity of the largest eddy. We assume that $\Delta v_I = \Delta v_{II}$ at the transition.

The size of dust aggregates determines how they interact with the gas. The dynamics of the aggregates is affected by their cross sections, which depend on their internal inhomogeneous structure. The radius of BCCA cluster a_{BCCA} consisted of N monomers ($N = m_d/m_0$) is given as $a_{BCCA} \simeq N^{0.5}a_0$ for $N \gg 1$ (Mukai et al. 1992; Wada et al. 2008, 2009), which was also confirmed through N -body simulations (Suyama et al. 2012). We then assume that

$$a_d(m_d) = \begin{cases} \left(\frac{m_d}{m_0}\right)^{1/2} a_0 & (BCCA) \\ \left(\frac{3m_d}{4\pi\rho_{int}}\right)^{1/3} & (otherwise). \end{cases} \quad (9)$$

2.2.2. Compression stages

The hit-and-stick stage ends due to collisions between the aggregates (collisional compression), or due to their interaction with the ambient gas (gas-drag compression). In the collisional compression, the rolling energy E_{roll} , which is the energy required to rotate a particle around a connecting point by 90° , is comparable to the impact energy, $E_{imp} = m_d \Delta v^2 / 4$, between the two porous dust aggregates of the same mass, m_d . Beyond this point, the aggregates start to get compressed due to mutual collisions and interaction with the gas (i.e., the ram pressure).

According to [Suyama et al. \(2012\)](#), the internal density of the aggregated $\rho_{int,f}$ formed by collisions between two equal-mass aggregates, with density ρ_{int} , is calculated for $E_{imp} > 0.45E_{roll}$:

$$\rho_{int,f} = \left(\rho_{int}^4 + \rho_f^4 \frac{E_{imp} - 0.45E_{roll}}{0.15N E_{roll}} \right)^{1/4}, \quad (10)$$

ρ_f is the fractal density of the dust aggregate: $\rho_f \approx m_d / (7.7a_d^{2.5})$, and $E_{roll} = 4.37 \times 10^{-9}$ erg.

Moreover, the fluffy dust aggregates can be compressed owing to the ram pressure of the ambient gas ([Kataoka et al. 2013](#)). The internal density of the aggregates that are compressed by the gas is given

$$\rho_{int,drag} \simeq \left(\frac{a_0^3}{E_{roll}} P_g \right)^{1/3} \rho_0, \quad (11)$$

where the ram pressure for a dust aggregate is

$$P_g = \frac{m_d v_d}{\pi a_d^2 t_s}, \quad (12)$$

with the stopping time $t_s = S_t / \Omega_K$ ([Kataoka et al. 2013](#)).

As the aggregates become more massive ($m_d > 10^{10}$ g), they start getting compressed owing to their self-gravity, and the internal density evolves as $\rho_{int} \propto (\Delta v)^{3/5} m_d^{-1/5}$ ([Okuzumi et al. 2012](#)).

2.2.3. *N*-body stage

When $S_t \simeq 1$, kinematics of the aggregates is affected not only by the turbulence, but also by mutual interaction between the aggregates as a *N*-body system and by the gravitational interaction with the density fluctuation due to the turbulence. Then the collision velocity between the aggregates is determined by a balance between various heating and cooling processes as the *N*-body particles. According to [Michikoshi, & Kokubo \(2016, 2017\)](#), we solve the following equation to get the equilibrium random velocity of the dust aggregates v_d ,

$$\begin{aligned} \frac{dv_d^2}{dt} = & \left(\frac{dv_d^2}{dt} \right)_{grav} + \left(\frac{dv_d^2}{dt} \right)_{turb,stir} + \left(\frac{dv_d^2}{dt} \right)_{turb,grav} \\ & - \left(\frac{dv_d^2}{dt} \right)_{coll} - \left(\frac{dv_d^2}{dt} \right)_{drag} = 0. \end{aligned} \quad (13)$$

The first three heating terms represent the gravitational scattering of the aggregates, stirring by the turbulence, and gravitational scattering by density fluctuation of the turbulence, respectively. The two cooling terms in eq.(13) represent the collisional damping and the gas drag. We assume the collision velocity $\Delta v \approx v_d$ at $S_t = 1$ and numerically solve eq. (13) in this stage.

2.2.4. Radial drift of the dust particles

In Paper I, we ignored the radial drift of the dust particles in the disk. However, as mentioned in §1, this is not always obvious. Here, we solve the following governing equations for the dust evolution based on the assumption that the mass distribution of the dust particles at each orbit radius is singly peaked at a mass (Tsukamoto et al. 2017; Sato et al. 2016);

$$\frac{\partial \Sigma_d}{\partial t} + \frac{1}{r} \frac{\partial}{\partial r} (r v_{r,d} \Sigma_d) = 0, \quad (14)$$

$$\frac{\partial m_d}{\partial t} + v_{r,d} \frac{\partial m_d}{\partial r} = \frac{m_d}{t_{coll}}. \quad (15)$$

Here t_{coll} in eq.(15) is the collision time, and the source term is

$$\frac{m_d}{t_{coll}} = m_d (4\pi a_d^2 n_d \Delta v) = 2\sqrt{2\pi} a_d^2 \Sigma_d \Delta v H_d^{-1}, \quad (16)$$

where n_d is the number density of the dust particles.

The dust particles have a radial velocity due to the drag with the ambient gas:

$$v_{r,d} = - \left(\frac{v_{r,g}}{1 + S_t^2} + \frac{2S_t}{1 + S_t^2} \eta v_K \right), \quad (17)$$

where v_K is the Kepler velocity and η is a parameter that determines the sub-Keplerian motion of the gas, and the radial velocity of the gas $v_{r,g}$ is given with the mass accretion rate \dot{M} :

$$v_{r,g} = - \frac{\dot{M}}{2\pi r \Sigma_g}, \quad (18)$$

where the mass accretion rate \dot{M} is assumed to be using the Eddington mass accretion rate $\dot{M} = \gamma_{Edd} \dot{M}_{Edd}$ with the Eddington ratio γ_{Edd} .

2.3. Gravitational instability of the dust disk and formation of planets

We investigate the gravitational instability (GI) of the disk consisting of dust aggregates with $S_t > 1$ using the Toomre's Q -value defined as

$$Q_d \equiv \frac{(v_d/\sqrt{3})\Omega_K}{3.36G\Sigma_d}. \quad (19)$$

For the axi-symmetric mode, $Q_d < 1$ is the necessary condition for GI, but the non-axisymmetric mode can develop for $Q_d \lesssim 2$. In this case, spiral-like density enhancements are formed followed by fragmentation of the spirals (Michikoshi, & Kokubo 2017), which leads formation of massive objects, i.e., *blanets*. The mass of blanets is estimated as

$$M_{bl} \simeq \lambda_{GI}^2 \Sigma_d, \quad (20)$$

where the critical wavelength for GI is

$$\lambda_{GI} = \frac{4\pi^2 G \Sigma_d}{\Omega_K^2}. \quad (21)$$

2.4. Initial and boundary conditions

In all the models, the circumnuclear cold gas disk embedded in the geometrically thick torus (see Fig. 1) is assumed to be gravitationally stable; the Toomre's Q-value, $Q_g \equiv c_s \Omega_K / \pi G \Sigma_g = 2$. The gas sound velocity is assumed to be $c_s^2 = k_B T_g / \mu m_H$ with $T_g = 100$ K and $\mu = 2.0$.

The Eddington ratio is assumed to be $\gamma_{Edd} = 0.01$. The AGN bolometric luminosity is then $L_{bol} = 1.3 \times 10^{42} \text{ erg s}^{-1} M_{BH} / (10^6 M_\odot)$. The X-ray luminosity of the AGN, which is used to determine the snowline radius, $L_X = 0.1 L_{bol}$. This can be attributed to the fact that the UV flux from the accretion disk is attenuated in the dense circumnuclear disk.

The snowline for $a_d = 0.1 \mu m$,

$$r_{snow} \approx 1.5 \text{ pc} \left(\frac{L_X}{1.3 \times 10^{41} \text{ erg s}^{-1}} \right)^{1/2} \left(\frac{T_{ice}}{170 \text{ K}} \right)^{-2.8} \left(\frac{a_d}{0.1 \mu m} \right)^{-1/2}. \quad (22)$$

Therefore, it is expected that the dust in the most part of the circumnuclear disk is icy. We assume $T_{ice} = 170$ K. The dust to gas mass ratio is assumed as $f_{dg} = 0.01$. We solve the governing equations (§2.2.4) between $r = 0.1$ pc and 200 pc with 600 grid cells.

3. RESULTS

Figure 2a shows a typical evolution of a dust aggregate at the snowline for $M_{BH} = 10^6 M_\odot$ and $\alpha = 0.02$. The internal density of the aggregate ρ_{int} is plotted as a function of its mass m_d . Initially, the internal density decreases monotonically from the monomer's initial density, i.e., $\rho_0 = 1 \text{ g cm}^{-3}$ to $4 \times 10^{-6} \text{ g cm}^{-3}$, as its mass increases from $m_d \sim 10^{-15} \text{ g}$ to $\sim 10^{-5} \text{ g}$. At that instant, the size of the aggregate becomes $\sim 1 \text{ cm}$ (see Fig. 2b). After this hit-and-stick phase, the fluffy dust aggregates keep growing due to collisions in the turbulent gas motion until $S_t \simeq 1$. During this stage ($m_d = 10^{-5} \text{ g}$ to 10^{10} g), the aggregates are compressed mainly due to the gas drag (§2.2.2), and therefore ρ_{int} gradually increases⁶. After $S_t \gtrsim 1$, the aggregates

⁶ The effect of the collisional compression is negligibly small in this case.

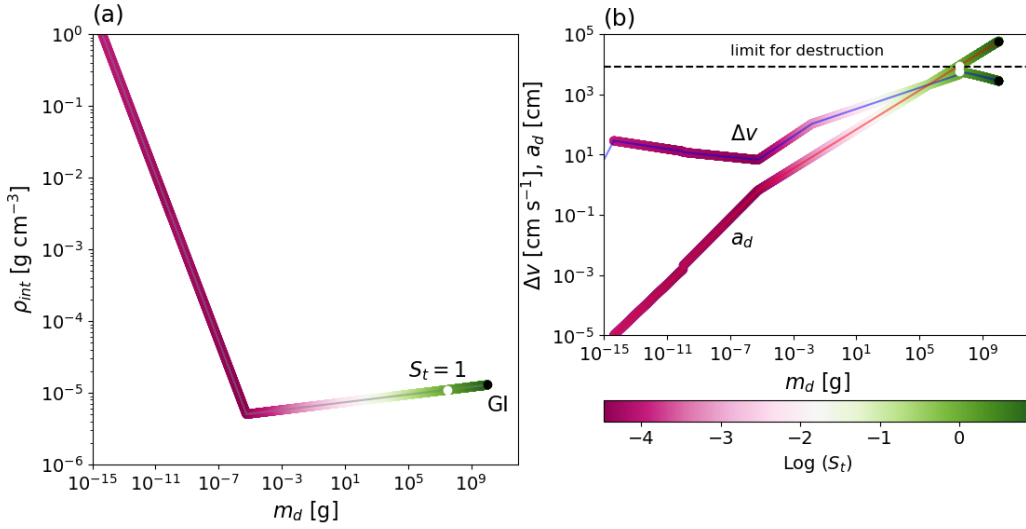


Figure 2. (a) Evolution of the internal density of a dust aggregate ρ_{int} at the snowline ($r = 1.5$ pc) as a function of the aggregate mass m_d for $M_{BH} = 10^6 M_\odot$ and $\alpha = 0.02$. Evolution prior to the gravitational instability (i.e., $Q_d > 2$) is plotted. The positions where S_t becomes unity and $Q_d = 2$ are shown by the filled white and black circles, respectively. The color bar represents the Stokes number.

(b) Same as (a), but for collision velocity of the aggregates Δv and size of the aggregate a_d . The dashed line shows $\Delta v = 80$ m s $^{-1}$, which is the limit for the collisional destruction of the aggregates suggested by numerical experiments (Wada et al. 2009). After $S_t = 1$ is attained, Δv drops and the disk of the aggregates becomes gravitationally unstable.

behave as a N -body system under the effect of the turbulent fluctuation (eq. (13)). For $m_d > 10^{10}$ g and $S_t > 1$, the aggregates are compressed due to their self-gravity. In the model shown in Fig. 2, it becomes gravitationally unstable at $t = 75$ Myr (see also §4.1).

Figure 2b plots the collisional velocity Δv of the aggregate and its size a_d as a function of m_d . The size a_d monotonically increases. In the compression stage ($m_d > 10^5$ g), the increase of a_d slows down (see eq.(9)). Initially Δv is 20 cm s $^{-1}$, and it slightly decreases during the hit-and-stick stage. Then it turns to an increase phase until ~ 57 m s $^{-1}$ around $S_t = 1$ during the compression stage. The size of the aggregate becomes $a_d \sim 10^4$ cm at the end of this stage. In this case, the aggregates are not compressed by their self-gravity ($m_d < 10^{10}$ g) before the dust disk becomes GI. Note that the increase of Δv slows down at $m_d \sim 0.1$ g, which corresponds to the transition between Δv_I and Δv_{II} (eqs. (7) and (8)).

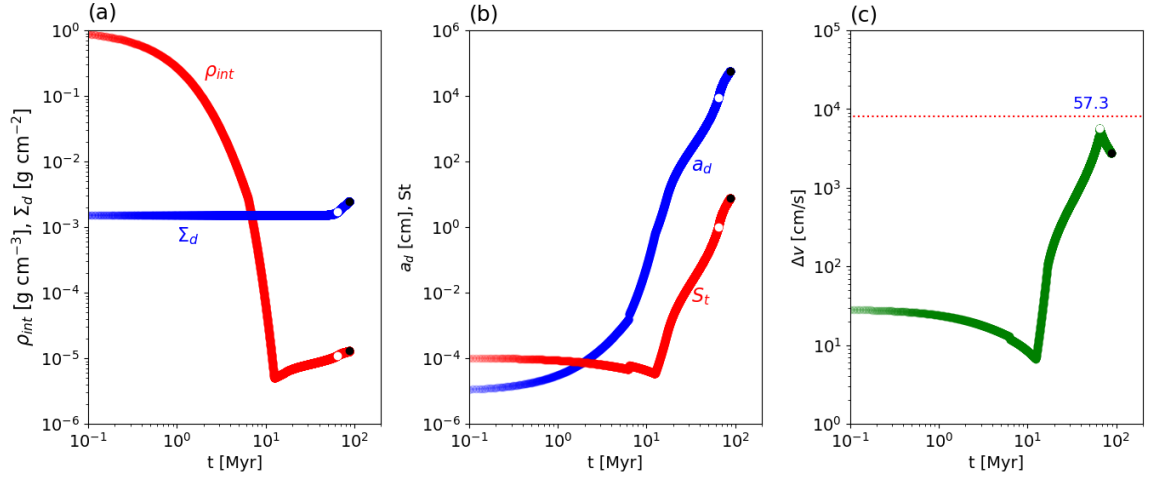


Figure 3. Time evolution of the internal density of the aggregate ρ_{int} , size a_d and collision velocity Δv for the same model shown in Fig. 2. Evolution prior to the gravitational instability is plotted. The position where $St = 1$ for each quantity is shown by a white filled circle. The maximum Δv is shown (57.3 m s^{-1} in this case) and the critical velocity for the collisional destruction (i.e., 80 m s^{-1}) is shown by the red-dotted line in panel (c).

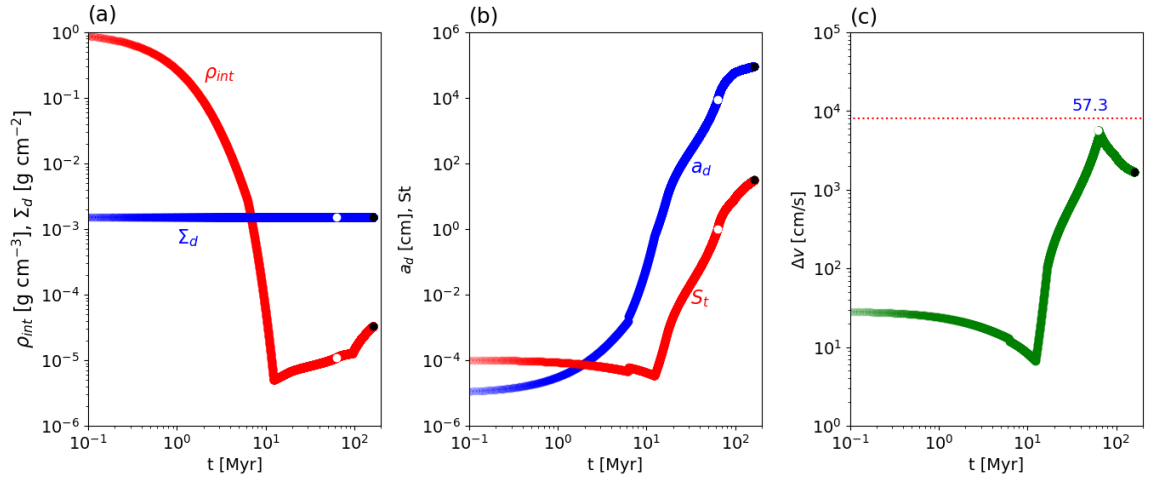


Figure 4. Same as Fig. 3, but the model *without* the radial drift of the dust. Note that the time of GI is 136 Myr, in contrast to 71 Myr in Fig. 3.

The growth time of an aggregate for $\Delta v = \Delta v_I \simeq 1/2\sqrt{\alpha}c_s R_e^{1/4} S_t$ can be estimated as

$$\begin{aligned} t_{grow} &\equiv \left(\frac{d \ln m_d}{dt} \right)^{-1} = \frac{4\sqrt{2\pi} H_d \rho_{int} a_d}{3 \Delta v \Sigma_d} \\ &\simeq \frac{16}{3} \sqrt{\frac{2}{\pi}} \frac{H_g}{\sqrt{\alpha} R_e^{1/4} c_s f_{dg}} \\ &\simeq 2.9 \times 10^7 \text{ [yr]} c_{s,1}^{-1} \left(\frac{f_{dg}}{0.01} \right)^{-1} \left(\frac{H_g}{0.1 \text{ pc}} \right) \left(\frac{\alpha}{0.02} \right)^{-1/2} \left(\frac{R_e}{10^4} \right)^{-1/4}. \end{aligned} \quad (23)$$

Figure 3 shows time evolution of ρ_{int} , a_d , S_t , and Δv for the same model shown in Fig. 2. The hit-and-stick phase lasts for ~ 10 Myr as expected by t_{grow} , and S_t becomes unity at $t = 60$ Myr. At this moment, the dust aggregate's size reaches ~ 100 m (Fig. 3b).

Fig. 3b shows that the growth of a_d is exponential, or slower in time, in contrast to the results in Paper I. This is a natural consequence of the evolution of the mass of the dust aggregates. The mass increase rate of the dust is

$$\frac{dm_d}{dt} \sim n_d a_d^2 \Delta v \sim \frac{\Sigma_d}{H_d} a_d^2 \Delta v \propto S_t^{1/2} a_d^2 \Delta v. \quad (24)$$

Here we assume the dust layer is sedimented, i.e., its thickness H_d is scaled as $H_d \propto S_t^{-1/2}$. For $\Delta v \propto S_t^{1/2}$ (eq. (8)), $dm_d/dt \propto m_d$, therefore, m_d grows exponentially. The runaway growth seen in Paper I is caused by the assumption that the internal density of the dust aggregates stays porous (i.e., the fractal dimension is ~ 2) through the evolution. In reality, when the compression by the ambient gas works, ρ_{int} is nearly constant (i.e., $m_d \propto a_d^3$), as shown in Fig. 2, therefore $S_t \propto a_d$. If the scale height of the dust disk is constant, then $dm_d/dt \propto S_t^{1/2} a_d^2 \propto m_d^{5/6}$; therefore, the growth of the dust aggregate should be slower than $\exp(t)$.

Fig. 3c shows that the collisional velocity Δv gradually decreases during the hit-and-stick stage, and it turns to rapid increase during the compression stage until S_t becomes unity at $t = 56$ Myr. In the N -body stage, the collisional velocity decreases from its maximum value, 57 m s^{-1} , and it becomes GI (i.e., $Q_d \leq 2$) at $t \simeq 75$ Myr.

For comparison, the evolution of the model without the radial drift is shown in Fig. 4. We found that the dust aggregates before $S_t = 1$ evolve almost the same way as that in the model with the radial drift (Fig. 3). However, the time for GI is 136 Myr, in contrast to 71 Myr for the case with the advection.

Figure 5 shows the radial distributions of Σ_d , H_d , Δv , the radial velocity of the dust and gas ($v_{r,d}$ and $v_{r,g}$), ρ_{int} , S_t , m_d , and a_d at 200 Myr in the same model shown in Fig. 2. As Fig. 5a shows, the dust is accumulated around $r \sim 2 - 3$ pc, where $v_{r,d} \ll v_{r,g}$ (Fig. 5c) and S_t turns from $S_t < 1$ to $S_t > 1$ (Fig. 5b). From Fig. 5d, the dust aggregates evolve more rapidly in the inner region ($r \lesssim 3$ pc), and the maximum size is $\sim \text{km}$. We call these objects as *blanetesimals*.

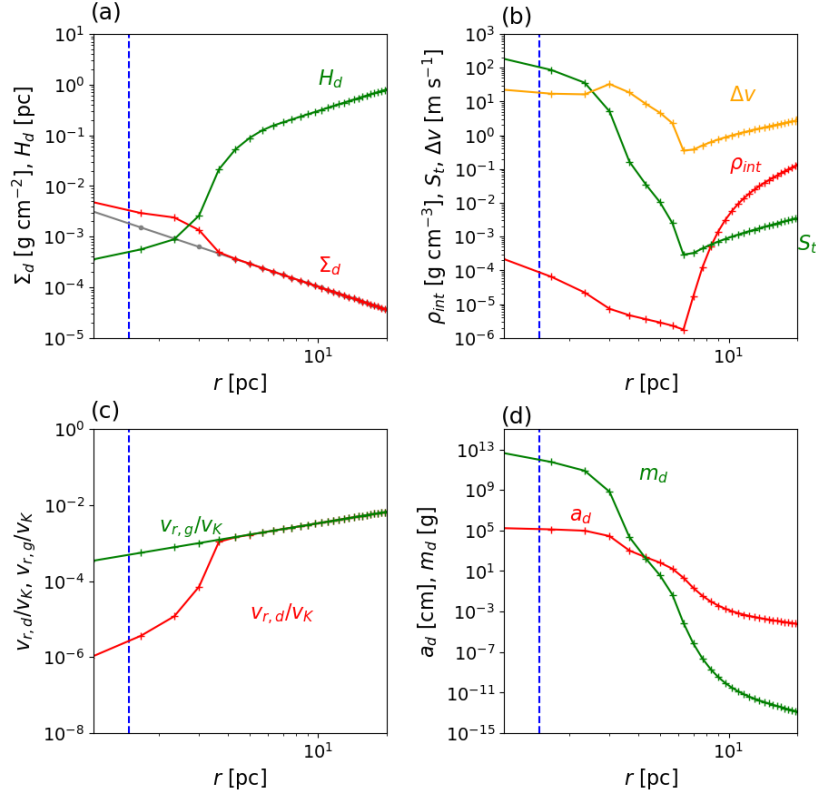


Figure 5. Radial distribution of various quantities at $t = 200$ Myr for the same model shown in Fig. 2. (a) Surface density of dust Σ_d and the scale height of the dust H_d . The gray line is Σ_d at $t = 0$. Note that the surface density of the dust decreases in the outer disk ($r > 30$ pc), and the total mass of the dust is conserved. The vertical dashed line is the position of the snowline $r_{snow} = 1.5$ pc. (b) Same as (a), but for the collision velocity Δv , the internal density of the aggregate ρ_{int} and the Stokes parameter S_t . (c) Same as (a), but for the radial velocity of the dust $v_{r,d}$ and $v_{r,g}$ normalized by the Kepler velocity v_K . (d). Same as (a), but for the mass and size of the aggregate, m_d and a_d .

4. DISCUSSION

4.1. Dependence on α and M_{BH} .

In the models with the radial drift of the dust aggregates, we investigated how the maximum velocity of the collision Δv_{max} and the time for GI (τ_{GI}) depend on α and M_{BH} . In Figure 6, we plot Δv_{max} and τ_{GI} as a function of α for $M_{BH} = 10^6 M_\odot$ and $10^7 M_\odot$. It shows that Δv_{max} depends on α , and not on M_{BH} . If $\Delta v_{max} \lesssim 80 \text{ m s}^{-1}$ is necessary for collisional growth as numerical experiments suggested (Wada et al. 2009), then α should be ~ 0.04 or smaller.

The behavior of the dust growth (e.g., Fig. 2) does not significantly depend on α and M_{BH} , but the timescale to reach $S_t = 1$ is different as shown in Fig. 6b. For example, for $M_{BH} = 10^6 M_\odot$ and $\alpha = 0.02$, it takes ~ 60 Myr when S_t exceeds unity,

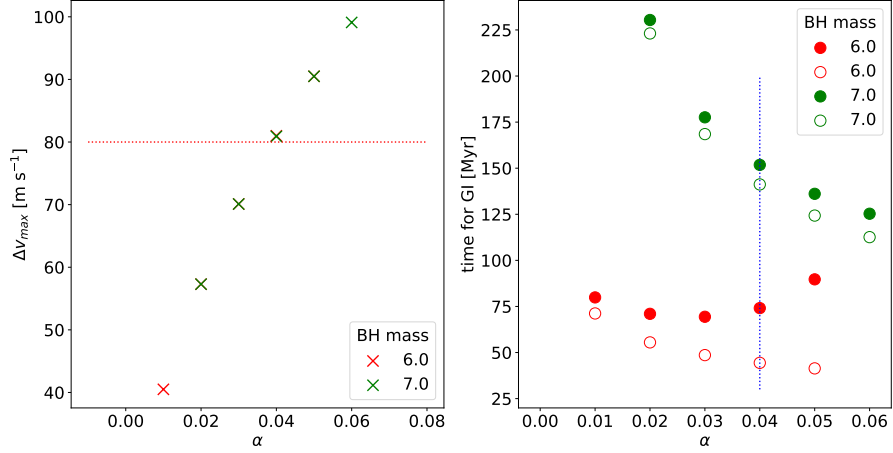


Figure 6. (a) Δv_{max} as a function of α in the models with the radial drift. Red and green crosses are $M_{BH} = 10^6 M_\odot$ and $10^7 M_\odot$, respectively. The dotted line is the velocity limit for collisional destruction (80 m s^{-1}). (b) Time for the gravitational instability (GI) as a function of α . The filled circles are the time for GI and the open circles are the time for $S_t = 1$. Red and green circles are $M_{BH} = 10^6 M_\odot$ and $10^7 M_\odot$, respectively. The α corresponds to $\Delta v_{max} = 80 \text{ m s}^{-1}$, i.e. $\alpha = 0.04$ is shown by the blue dotted line.

whereas it is $\sim 225 \text{ Myr}$ for $M_{BH} = 10^7 M_\odot$ and $\alpha = 0.02$. This implies that smaller BHs may preferentially host blanets within a lifetime AGNs ($\lesssim 10^8 \text{ yr}$). Figure 6b shows that, for $M_{BH} = 10^7 M_\odot$, the blanetesimal disk may not become GI earlier than $\sim 150 \text{ yr}$ for $\alpha < 0.04$. For $\alpha > 0.05$ or 0.06 , GI does not occur at $r = r_{snow}$ in the models with $M_{BH} = 10^6 M_\odot$ or $10^7 M_\odot$, respectively.

4.2. Number and mass of blanets

In the final stage of the evolution, the *blanetesimal* disk can be gravitationally unstable, and it fragments into massive objects, i.e., *blanets* (see §2.3). Figure 7 shows the radial distribution of the mass and typical separation between blanets, $\lambda_{bl} \approx \lambda_{GI}$ (eq.(21)). Two models with the radial drift for $M_{BH} = 10^6 M_\odot$ with $\alpha = 0.02$ and $M_{BH} = 10^7 M_\odot$ with $\alpha = 0.04$ are shown. For comparison, a model without the radial drift is also shown ($M_{BH} = 10^6 M_\odot$ and $\alpha = 0.02$). The mass of blanets ranges from $\simeq 20 M_E$ at $r = r_{snow}$ to $\simeq 3000 M_E$ at $r \sim 3.5 \text{ pc}$ for $M_{BH} = 10^6 M_\odot$, in contrast to the model without advection, which is $M_{bl} \simeq 3 M_E - 7 M_E$. For $M_{BH} = 10^7 M_\odot$, $M_{bl} \gtrsim 10^4 M_E - 10^5 M_E$ outside the snowline. However, this extraordinary massive blanet is unlikely, because it is comparable to the minimum mass of brown dwarfs ($\sim 2 \times 10^4 M_E$). Therefore, the largest size of the blanets (R_{bl}) would be maximally $\sim 10 \times$ Earth’s radius at $r \sim 3 \text{ pc}$ for $M_{BH} = 10^6 M_\odot$, if the average internal density is similar to that of the Earth.

Number of blanets is $\sim 8 \times 10^5$ at $r = r_{snow}$ for $M_{BH} = 10^6 M_\odot$ with $\alpha = 0.02$, provided that all the dust is converted to blanets through GI. From Fig. 7, the average distance between blanets would be $\lambda_{bl} \sim 10^{-3} \text{ pc}$ at $r = r_{snow}$. Therefore, the

system of blanets does not resemble any known exoplanet systems, in a sense that the “planets” are isolated, dominant objects in their orbits.

Is the swarm of blanets the final form of the system? The collisional time scale t_{coll} for the blanets can be estimated as:

$$t_{coll}^{-1} = 4\sqrt{\pi} n_{bl} \sigma_{bl} \left(r_{coll}^2 + \frac{G m_{bl}}{\sigma_{bl}^2} r_{coll} \right), \quad (25)$$

where where n_{bl} and σ_{bl} are the number density and velocity dispersion of the blanets, respectively. r_{coll} is the distance at the closest approach, which is $r_{coll} \sim 2R_{bl}$ (Binney, & Tremaine 2008). The second term of eq. (25) represents the gravitational focusing, which enhances the collision rate. For $n_{bl} \sim \lambda_{bl}^{-3} \simeq (10^{-3} \text{ pc})^{-3}$, $M_{bl} \simeq 20M_E$, $R_{bl} \simeq 3R_E$, and $\sigma_{bl} \sim \Delta v \simeq 30 \text{ m s}^{-1}$ (Fig. 3c), the collisional time is $t_{coll} \approx 6 \text{ Gyr}$. This can be shorter, if three-body encounters between a close-binary and a blanet are considered. Therefore, the blanet system could dynamically evolve in the cosmological time scale, and it would be interesting study the evolution by direct N -body simulations.

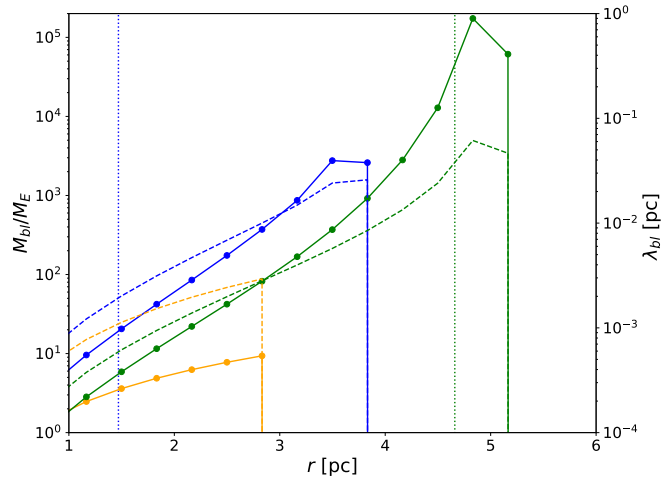


Figure 7. Radial distribution of mass in the Earth mass M_E (solid lines) for the left vertical axis, and the critical wave length for GI (λ_{bl}) by the dashed lines for the right vertical axis. The advection models for $M_{BH} = 10^6 M_\odot, \alpha = 0.02$ (blue) and $M_{BH} = 10^7 M_\odot, \alpha = 0.04$ (green) are shown in blue and green lines, respectively. The model without advection ($\alpha = 0.02$) is shown by orange lines. The blue and green vertical dotted lines are position of snowlines for $M_{BH} = 10^6 M_\odot$ and $M_{BH} = 10^7 M_\odot$, respectively.

4.3. Can blanets acquire a massive gas envelope?

It would be interesting to investigate whether blanets can obtain an atmosphere. If the Hill radius r_H of a blanet is larger than the disk scale height, the blanets may form a gap, then the obtained mass of the atmosphere depends on r_H . The Hill radius

of a planet, $r_H = (M_{bl}/3M_{BH})^{1/3} r$ is

$$r_H \simeq 10^{-4} \text{ pc} \left(\frac{M_{bl}}{1000 M_E} \right)^{1/3}, \quad (26)$$

whereas the scale height of the gas disk at $r = 1.5 \text{ pc}$ for $M_{BH} = 10^6 M_\odot$ is, $H_g \simeq c_s/\Omega_K \simeq 2 \times 10^{-2} M_{BH,6}^{-1/2} \text{ pc}$, which is larger than r_H .

On the other hand, the Bondi radius is

$$r_B \equiv \frac{GM_{bl}}{c_s^2} \simeq 1.3 \times 10^{-5} \text{ pc} \left(\frac{M_{bl}}{1000 M_E} \right) \left(\frac{c_s}{1 \text{ km s}^{-1}} \right)^{-2}. \quad (27)$$

Therefore, we suspect that the mass of the atmosphere is limited by the Bondi accretion, rather than by a gap formation. If this is the case, the envelope mass would be

$$M_{env} \sim \frac{4\pi}{3} r_B^3 \rho_g \quad (28)$$

$$\approx 10^{-7} M_E \left(\frac{M_{bl}}{1000 M_E} \right)^3 \left(\frac{c_s}{1 \text{ km s}^{-1}} \right)^{-6} \left(\frac{\rho_g}{2 \times 10^{-21} \text{ g cm}^{-3}} \right). \quad (29)$$

However, if the Bondi radius is filled with the ambient gas during the orbital motion of a planet, the envelope mass could be maximally

$$M_{env} \sim 2\pi r_{bl} \cdot \pi r_B^2 \rho_g \sim 0.05 M_E, \quad (30)$$

for $M_{bl} = 1000 M_E$ at $r_{bl} = 1.5 \text{ pc}$. The small M_{env} would suggest that the runaway accretion of the gas to planets and formation of massive “gas giants” are difficult, but it also depends on how quickly are the orbits of planets filled with the gas. This is an interesting open question for future studies.

4.4. *Can other mechanisms of planet formation be applicable?*

In this paper, we focused on the evolution of the dust aggregates based on the coagulation theories of dust monomers and the gravitational instability. Other formation mechanisms of planetesimals have also been proposed and extensively discussed in the planet formation community. Among them, we here look over the pebble accretion, secular gravitational instability (secular GI), and the streaming instability as possible mechanisms of planetesimal formation. More quantitative analysis in the circumnuclear environment would be interesting for future studies.

The pebble accretion is an accretion process of small solid bodies (i.e., pebbles) to massive seed objects (e.g., planets or planetesimals) under the effect of the gas drag and gravity (e.g., Ormel 2017; Lambrechts et al. 2019). In the present case, relatively massive aggregates could accumulate ambient smaller particles, then they could become more massive. However, the time scale conditions for the pebble accretion (Ormel & Liu 2018), i.e., $t_{settl} < t_{enc}$ and $t_{stop} < t_{enc}$ are not likely to be satisfied in

the circumnuclear disk, where the settling time t_{settl} is the time needed for a particle to sediment to the massive objects, and the encounter time t_{enc} is the duration of the gravitational encounter time. In other words, the radial flux of pebbles due to the gas drag is too small in the region of $S_t \ll 1$. Moreover, the relatively large turbulent motion of the gas (i.e., $\alpha \gtrsim 0.01$) may prevent from the pebble accretion (Ormel & Liu 2018), in contrast to the circumstellar disk. Therefore, we do not expect that the pebble accretion is a major process as a formation mechanism of blanets.

The secular GI, which is the gravitational instability due to gas-dust friction, is another possible mechanism to form planets in the circumstellar disk (Youdin 2011). According to Takahashi & Inutsuka (2014), the condition for this instability is expressed as

$$\Gamma \equiv \left(\frac{\alpha}{4 \times 10^{-5}} \right) \left(\frac{f_{dg}}{0.1} \right)^{-2} \left(\frac{Q_g}{10} \right) \left(\frac{\eta}{0.01} \right) \lesssim 1. \quad (31)$$

In the present case, $\Gamma \sim 100$ for $\alpha \gtrsim 0.01$, $f_{dg} = 0.01$, $\eta \sim 10^{-4}$ and $Q_g = 2$, therefore we do not expect the secular GI in the circumnuclear disk.

The streaming instability could be an effective mechanism to make condensations of dust particles, if the dust-to-gas mass ratio (f_{dg}) is close to unity (e.g. Youdin & Goodman 2005). According to numerical simulations by Carrera et al. (2015), coagulation of particles driven by the streaming instability depends on f_{dg} and S_t . They found that the streaming instability occurs for $f_{dg} \sim 0.02$ for $S_t \sim 0.1$. In our case, the dust-to-gas mass ratio increases to $f_{dg} \simeq 0.02 - 0.03$ from the initial value (0.01) outside the snowline due to the radial drift of the dust aggregates. However, $S_t \gg 1$ in the region (Fig. 5b), therefore we do not expect that the streaming instability occurs in the circumnuclear disk.

5. SUMMARY

In this follow-up paper of Wada et al. (2019) (Paper I), we theoretically investigated a process of dust evolution around a SMBH in the galactic center. We proposed that a new class of astronomical objects, *blanets* can be formed, provided that the standard scenario of planet formation is present in the circumnuclear disk.

Here, we investigated the physical conditions of the blanet formation outside the snowline ($r_{snow} \sim$ several parsecs) in more detail, especially considering the effect of the radial drift of the dust aggregates. We also improved the dust evolution model in Paper I in terms of the internal density evolution of the dust aggregates. We assumed the maximum collisional velocity for destruction, which was suggested by previous numerical simulations, as one of necessary conditions for blanet formation. We found that a dimensionless parameter $\alpha = v_t^2/c_s^2$, where v_t is the turbulent velocity and c_s is the sound velocity, describing the effective angular momentum transfer due to the turbulent viscosity in the circumnuclear disk should be smaller than 0.04 for the black hole mass $M_{BH} = 10^6 M_\odot$; otherwise, the dust aggregates could be destroyed

due to collisions. The formation timescale of blanets τ_{GI} at r_{snow} is $\tau_{GI} \simeq 70\text{-}80$ Myr for $\alpha = 0.01 - 0.04$. The blanets (M_{bl}) are more massive for larger radii; they range from $M_{bl} \sim 20M_E - 3000M_E$ in $r < 4$ pc, in contrast to $M_{bl} = 3 - 7M_E$ for the case without the radial drift.

The typical separations between the blanets, estimated from the wavelength of the gravitational instability, would be $\sim 10^{-3} - 10^{-2}$ pc.

For $M_{BH} \geq 10^7 M_\odot$, the formation timescale is longer than ~ 150 Myr for $\alpha \leq 0.04$. Although the gravitational instability of the blanetesimal disk takes place just outside the snowline ($r = 4.7$ pc), they should not be blanets because they are more massive than the typical brown dwarf mass ($\sim 3 \times 10^4 M_E$). Note that AGNs are often heavily obscured with dense gas even for hard X-rays (Buchner et al. 2014) ($N_H > 10^{23} \text{ cm}^{-2}$, i.e., Compton-thick). If this is the case, the snowline is located at the inner region (e.g. $r \sim 2 - 3$ pc), and as a result, blanets with $M_{bl} \sim 10M_E - 100M_E$ around $M_{BH} = 10^7 M_\odot$ could be possible. Our results suggest that *blanets* could be formed around relatively low-luminosity AGNs during their lifetime ($\lesssim 10^8$ yr). The system of *blanets* should be extraordinarily different from the standard Earth-type planets in the exoplanet systems. The blanets may acquire a rarefied atmosphere due to accretion of the gas in the circumnuclear disk (§4.3). The dynamical evolution of the swarm of blanets around a SMBH and whether they become more massive objects or destroyed due to collisions may be an interesting subject for future studies (§4.2).

ACKNOWLEDGMENTS

We would like to appreciate the anonymous referee's many valuable comments. The authors also thank Hidekazu Tanaka for many thoughtful comments. This work was supported by JSPS KAKENHI Grant Number 18K18774.

REFERENCES

- Barvainis, R. 1987, *ApJ*, 320, 537
- Buchner, J. Georgakakis, A., Nandra, K. et al. *A&Ap* 564, 125 (2014)
- Binney, J., Tremaine, S. "Galactic Dynamics 2nd. Edition", p. 626, Princeton University Press, Princeton (2008)
- Carrera, D., Johansen, A., & Davies, M. B. 2015, *A&A*, 579, A43.
doi:10.1051/0004-6361/201425120
- Greenhill, L. J., Booth, R. S., Ellingsen, S. P., et al. 2003, *ApJ*, 590, 162.
doi:10.1086/374862
- Izumi, T., Wada, K., Fukushige, R., et al. 2018, *ApJ*, 867, 48
- Kataoka, A., Tanaka, H., Okuzumi, S., et al. 2013, *A&A*, 557, L4
- Kudoh, Y., Wada, K., & Norman, C. 2020, arXiv:2008.07050
- Lambrechts, M., Morbidelli, A., Jacobson, S. A., et al. 2019, *A&A*, 627, A83.
doi:10.1051/0004-6361/201834229
- Michikoshi, S., & Kokubo, E. 2017, *ApJ*, 842, 61
- Michikoshi, S., & Kokubo, E. 2016, *ApJL*, 825, L28
- Mukai, T., Ishimoto, H., Kozasa, T., et al. 1992, *A&A*, 262, 315
- Netzer, H. 2015, *ARA&A*, 53, 365
- Okuzumi, S., Tanaka, H., & Sakagami, M.-aki . 2009, *ApJ*, 707, 1247
- Okuzumi, S., Tanaka, H., Kobayashi, H., et al. 2012, *ApJ*, 752, 106
- Ormel, C. W. 2017, *Formation, Evolution, and Dynamics of Young Solar Systems*, 197.
- Ormel, C. W., & Cuzzi, J. N. 2007, *A&A*, 466, 413
- Ormel, C. W. & Liu, B. 2018, *A&A*, 615, A178.
doi:10.1051/0004-6361/201732562
- Sato, T., Okuzumi, S., & Ida, S. 2016, *A&A*, 589, A15
- Schartmann, M., Wada, Keiichi, Prieto, M. A., Burkert, A., & Tristram, K. R. W. 2014, *MNRAS*, 445, 3878
- Shlosman, I., & Begelman, M. C. 1987, *Nature*, 329, 810
- Suyama, T., Wada, K., & Tanaka, H. 2008, *ApJ*, 684, 1310
- Suyama, T., Wada, Koji, Tanaka, H., et al. 2012, *ApJ*, 753, 115
- Takahashi, S. Z. & Inutsuka, S.-. ichiro . 2014, *ApJ*, 794, 55.
doi:10.1088/0004-637X/794/1/55
- Tsukamoto, Y., Okuzumi, S., & Kataoka, A. 2017, *ApJ*, 838, 151
- Wada, Koji., Tanaka, H., Suyama, T., et al. 2008, *ApJ*, 677, 1296
- Wada, K. & Norman, C. A. 2002, *ApJL*, 566, L21. doi:10.1086/339438
- Wada, Keiichi. 2012, *ApJ*, 758, 66
- Wada, Keiichi. 2015, *ApJ*, 812, 82
- Wada, Koji., Tanaka, H., Suyama, T., et al. 2009, *ApJ*, 702, 1490
- Wada, K., Tanaka, H., Okuzumi, S., et al. 2013, *A&A*, 559, A62
- Wada, Keiichi., Schartmann, M., & Meijerink, R. 2016, *ApJL*, 828, L19
- Wada, Keiichi., Fukushige, R., Izumi, T., & Tomisaka, K. 2018, *ApJ*, 852, 88
- Wada, K., Tsukamoto, Y., & Kokubo, E. 2019, *ApJ*, 886, 107 (Paper I)
- Weidenschilling, S. J. 1977, *MNRAS*, 180, 57
- Youdin, A. N. & Goodman, J. 2005, *ApJ*, 620, 459. doi:10.1086/426895
- Youdin, A. N., & Lithwick, Y. 2007, *Icarus*, 192, 588
- Youdin, A. N. 2011, *ApJ*, 731, 99.
doi:10.1088/0004-637X/731/2/99